Journal of Nuclear Materials 403 (2010) 25–31

Contents lists available at ScienceDirect

Journal of Nuclear Materials

journal homepage: www.elsevier.com/locate/jnucmat

Solubility studies and thermal expansion coefficient of uranium–lanthanum mixed oxide system

R. Venkata Krishnan, G. Panneerselvam, M.P. Antony, K. Nagarajan *

Fuel Chemistry Division, Indira Gandhi Centre for Atomic Research, Kalpakkam 603 102, Tamil Nadu, India

ARTICLE INFO

Article history:
Received 21 December 2009
Accepted 28 May 2010

ABSTRACT

Uranium–lanthanum mixed oxides $(U_{1-y}\ La_y)\ O_{2\pm x}$ ($y = 0.1$–0.9) of 13 different compositions were prepared by combustion synthesis using citric acid as the fuel. Sintering of the solid solutions was carried out at 1873 K. The solubility limit of La_2O_3 in UO_2 at 1873 K was determined to be ~82% from the room temperature XRD patterns of the sintered samples. However, the solubility limit of La_2O_3 in the mixed oxides prepared by solid-state route and sintered under identical conditions was found to be ~70%. The coefficients of thermal expansion for $(U_{1-y}\ La_y)\ O_{2\pm x}$ ($y = 0.2$, 0.4, 0.6, 0.8) in the temperature range 298–1973 K determined by high temperature X-ray diffraction (HTXRD) method are 17.7, 18.5, 19.2 and 20.0 $\times 10^{-6}\ K^{-1}$, respectively.

© 2010 Elsevier B.V. All rights reserved.

1. Introduction

The solid fission products formed during irradiation of oxide fuels in a fast reactor, could be classified into three categories viz., those forming metallic inclusions or oxide precipitates or solid solutions with the fuel matrix [1,2]. Rare-earth sesqui-oxides, Ln_2O_3 (Ln = La, Ce, Nd, Y, Sm, Gd or Eu) are known to be soluble in UO_2 lattice [3–5]. The extent of solubility of lanthanum oxide in UO_2 lattice depends on factors such as temperature, O/M, ambient conditions during heat treatment (oxidizing reducing or vacuum) etc. [6–12]. The results are consolidated and reported in a review article [6]. There are large differences in the reported solubility limit data to form single phase FCC solid solution. Hence the determination of solid solubility of La_2O_3 in UO_2 was taken up in this study. Gel combustion synthesis also called self-propagating high temperature synthesis (SHS) is a technique used for the preparation of a variety of materials ranging from high-tech ceramics to intermetallics [13–16]. Large amount of gases evolved during the gel combustion synthesis results in formation of a product, which is highly porous, and whose particle size is in the range of nm [17]. It has been reported that the solid solubility of the materials in nanometer scale is very different from that of the materials of larger sizes [18–20] and that the kinetics of solid-state reaction is greatly enhanced with decrease in the grain size in nanometer region [21]. In the present work, the solid solubility of lanthanum oxide in UO_2 was determined by preparing the solid solutions through gel combustion as well as solid-state routes.

To the best of our knowledge, high temperature X-ray diffraction (HTXRD) based lattice thermal expansion data of (U, La) mixed oxides are not available in the literature. Therefore, HTXRD based thermal expansion measurements were carried out on $(U_{1-y}\ La_y)\ O_{2\pm x}$ ($y = 0.2$, 0.4, 0.6 and 0.8) in the temperature range 298–1973 K. The results of the solubility and thermal expansion measurements are discussed in this paper.

2. Experimental

2.1. Sample preparation

Lanthanum oxide of 99.9% purity supplied by M/s. Indian Rare Earths and uranium oxide of nuclear grade purity supplied by NFC, Hyderabad were used for preparing the samples. Solid solutions of $(U_{1-y}\ La_y)\ O_{2\pm x}$ ($y = 0.1$–0.9) were prepared by combustion synthesis using citric acid as fuel. UO_2 was heated in air at 873 K for 6 h to convert it to U_3O_8. La_2O_3 was heated in air at 673 K to remove any adsorbed moisture. Stoichiometric amounts of U_3O_8 and La_2O_3 were taken and dissolved in nitric acid by heating at around 353 K. Citric acid was then added to the nitrate solution and mixed to get a clear solution. Stoichiometric ratio of oxidant (nitrate) to fuel (citric acid) was used for the preparation. The solution was heated to dryness on a hot plate at 573 K. The combustion of the mixture took place with a flame. The solid mass obtained after combustion was powdered using mortar and pestle. The resultant

* Corresponding author. Address: Head Pyrochemical Processing Studies Section, Fuel Chemistry Division, Chemistry Group, Indira Gandhi Centre for Atomic Research, Kalpakkam 603 102, Tamil Nadu, India. Tel.: +91 44 27480500x24289; fax: +91 44 27480065.
E-mail address: knag@igcar.gov.in (K. Nagarajan).

0022-3115/$ - see front matter © 2010 Elsevier B.V. All rights reserved.
doi:10.1016/j.jnucmat.2010.05.026

fine powder was calcined at 1073 K in air for 4 h to remove carbonaceous material from the sample. The resultant fine powder was compacted into pellets using a hydraulic press at a compaction pressure of 500 MPa. The sample pellets were reduced by heating under flowing Ar + 8% H_2 gas mixture at 873 K. The pellets were sintered by heating at 1873 K for 6 h at a heating rate of 250 K h^{-1}. Before heating the samples, the furnace was evacuated to 10^{-3} mbar and filled with ultra high pure Ar + 8% H_2 gas mixture three times. The sample pellets were heated under flowing Ar + 8% H_2. The sintered samples prepared were stored in an argon atmosphere glove box containing less than 20 ppm of moisture and oxygen to prevent oxidation of the sample.

Three solid solutions $(U_{1-y}\ La_y)\ O_{2\pm x}$ (y = 0.6–0.8) were prepared by solid-state route. Stoichiometric amounts of U_3O_8 and La_2O_3 were ground thoroughly using mortar and pestle. The ground powder was pelletized along with a binder (polyethylene glycol). The pellet samples were calcined in air for 8 h at 873 K to remove the binder. Reduction and sintering procedure followed was the same as that used for the preparation of mixed oxide pellets by gel combustion route.

2.2. Compositional characterization

The concentrations of U and La in the samples were determined by high-pressure liquid chromatography (HPLC) and inductively coupled plasma atomic emission spectroscopy (ICP–AES) techniques as explained in our previous publications [22,23]. Standard samples of U and La were prepared by dissolving stoichiometric quantities of U_3O_8 and La_2O_3 in nitric acid and diluting to a concentration range of 5–100 ppm for HPLC analysis and 5–25 ppm for ICP–AES analysis. Similarly the mixed oxide samples were also dissolved in nitric acid and diluted. The concentrations of U and La were determined from the calibration plots. The samples were also subjected to scanning electron microscopy–energy dispersive analysis of X-ray (SEM–EDAX) study for homogeneity and compositional analysis using SEM XL 30 EFEM of M/s. Philips, Holland (W – electron source, operation at 30 kV, vacuum better than 6×10^{-5} torr, secondary electrons and back scattered electrons for image analysis and SiLi detector for elemental analysis).

The samples were analyzed for impurity using an inductively coupled plasma–mass spectrometrometer (ICP–MS) of model number ELAN 250 of M/s. Sciex, Canada (now Perkin Elmer). The samples were dissolved in conc. HNO_3 and slowly heated to evaporate the solution to dryness. The nitrates of uranium and lanthanum formed were dissolved in 4 M HNO_3 (quartz distilled) and the solutions thus obtained were equilibrated with TBP solution (30% TBP in dodecane) three times to remove uranium completely from the solution. The aqueous solution was then diluted as per the requirement and subjected to estimation of impurities using ICPMS. The samples were analyzed for carbon impurity by using carbon analyzer of M/s. Eltra, Germany (ELTRACS 800).

2.3. Structural characterization

Pellets of $(U_{1-y}\ La_y)\ O_{2\pm x}$ (y = 0.1–0.9) as well as those of pure La_2O_3 and $UO_{2.00}$, were powdered and characterized by XRD. The X-ray diffraction patterns were recorded in the range, $10^\circ < 2\theta < 80^\circ$. Peak positions and the relative intensities were computed using a peak-fit program of the Philips X'pert Plus® software. The calibration of the diffractometer was carried out using silicon and α-alumina standards. The XRD patterns of La_2O_3 and $UO_{2.00}$ agreed well with the literature data [24,25]. The lattice parameters (a) were estimated by considering the eight major reflections of the CaF_2 structure. Finally an effective high angle corrected lattice parameter at each temperature was obtained by the standard Nelson Riley extrapolation procedure.

2.4. Determination of O/M ratio

The O/M ratios of the mixed oxides were determined by spectrophotometric method as described in our previous publication [23].

2.5. Thermal expansion measurements

The thermal expansion characteristics of the samples were studied using HTXRD in the temperature range 298–1973 K. The HTXRD studies were performed in a Philips X'pert MPD® system, equipped with the Büehler® high vacuum heating stage. Typical instrument related parameters were: operating voltage of 40 kV; current of 45 mA for the X-ray tube; scan speed of 0.02 s^{-1} with a counting time of 6 s per step and an angular range (2θ) of 20–80°. The diffraction patterns of the sample holder made of tantalum was co-recorded along with the sample for internal temperature calibration. Calibration of the diffractometer was carried out using silicon and α-Al_2O_3 standards obtained from National Institute of Standards and Technology (NIST), USA. The heating stage consisted of a thin (~80 μm), resistance heated tantalum foil, on top of which the sample was placed. Temperature was measured by a *W–Re* thermocouple, which was spot-welded to the bottom of the tantalum heater and controlled to an accuracy of about ±1 K. Diffraction studies were performed using Cu Kα radiation in the Bragg–Brentano geometry, in steps of 100 K up to 1973 K. A heating rate of 1 K min^{-1} and a holding time of 60 min at each temperature of measurement were adopted. The specimen stage was purged with high purity helium three times before the start of every experimental run and a vacuum level of about 10^{-5} mbar was maintained throughout the experiment. Acquisition and preliminary analysis of data were performed by the Philips X'pert Plus® software, although at a latter stage, an independent processing of the raw data was carried out for a precise determination of the peak positions. Room temperature XRD pattern was again taken after the completion of thermal expansion measurements to confirm that no oxidation of the sample had taken place during measurement.

3. Results and discussion

3.1. Sample characterization

The results of the impurity analysis carried out by using ICP–MS and carbon analyzer are shown in Table 1. As seen from Table 1, the total impurity elements concentration in the $(U_{1-y}\ La_y)\ O_{2\pm x}$ solid solutions with y = 0.2 and 0.4 did not exceed 250 ppm whereas that for y = 0.6 and 0.8 was within 500 ppm. The relative composition of U and La in the solid solution determined by ICP–AES, HPLC and SEM–EDAX analysis is shown in Table 2. As seen in Table 2, results of compositional characterization show good agreement within ±1% of the expected values. The results on O/M (M = U + La) measurement of the solid solutions are shown in Table 3. For the estimation of homogeneity, SEM–EDAX was performed on 10 different locations within the pellet and it was found that the sample pellets are extremely homogeneous. The room temperature XRD patterns of $(U_{1-y}\ La_y)\ O_{2\pm x}$ (y = 0.1–0.9) are shown in Fig. 1. The estimated O/M (M = U, La), lattice parameter and the phases present in the solid solutions prepared by combustion as well as by solid-state route are listed in Table 3.

3.2. Solubility studies

The room temperature XRD patterns of $(U_{1-y}\ La_y)\ O_{2\pm x}$ (y = 0.1–0.9) of Fig. 1 show that the $(U_{1-y}\ La_y)\ O_{2\pm x}$ (y = 0.1–0.8) solid

Table 1
Impurity analysis of (U, La) mixed oxides using ICP–MS.

Elements	$(U_{0.8}La_{0.2})$ $O_{1.95}$	$(U_{0.6}$ $La_{0.4})$ $O_{1.87}$ (ppm)	$(U_{0.4}$ $La_{0.6})$ $O_{1.87}$	$(U_{0.2}$ $La_{0.8})$ $O_{1.71}$
Ni	7	6	6	2
Zn	3	2	2	4
Mo	13	3	3	149
Ba	<1	<1	6	12
Al	<1	<1	2	2
Mg	<1	<1	<1	<1
Ca	<1	22	3	13
V	<1	<1	<1	<1
Cr	9	7	6	4
Mn	1	1	2	2
Fe	32	32	127	129
Cu	<1	<1	2	<1
Ce	11	1	5	12
Nd	<1	6	35	4
Sm	<1	<1	1	<1
Eu	<1	<1	<1	2
Gd	8	25	21	3
Dy	<1	<1	<1	<1
C	<100	<100	<100	<100

Table 2
Relative composition of U and La determined by ICP–AES, HPLC and SEM–EDAX.

Method	ICP–AES		HPLC		SEM–EDAX	
Mixed oxide	U/%	La/%	U/%	La/%	U/%	La/%
$(U_{0.8}La_{0.2})$ $O_{1.95}$	79.8	20.2	80.1	19.9	80	20
$(U_{0.6}$ $La_{0.4})$ $O_{1.87}$	60.3	39.7	60.1	39.9	61	39
$(U_{0.4}$ $La_{0.6})$ $O_{1.87}$	39.9	60.1	40.2	59.8	40	60
$(U_{0.2}$ $La_{0.8})$ $O_{1.71}$	20.2	79.8	20.1	79.9	20	80
$(U_{0.18}$ $La_{0.82})$ $O_{1.69}$	18.1	81.9	17.9	82.1	18	82

Table 3
X-ray and chemical analysis of urania-lanthana solid solutions prepared by combustion and by solid-state route.

Compound	O/U	O/M	Lattice parameter/nm	Phases present
$UO_{2.00}$	2.00	2.00	0.5468	FCC
La_2O_3	0	1.5	a = 0.3936 c = 0.6133	HXL
Solid solution prepared by combustion synthesis				
$(U_{0.9}$ $La_{0.1})$ oxide	2.055	1.999	0.5476	FCC
$(U_{0.8}$ $La_{0.2})$ oxide	2.065	1.952	0.5488	FCC
$(U_{0.7}La_{0.3})$ oxide	2.090	1.913	0.5503	FCC
$(U_{0.6}$ $La_{0.4})$ oxide	2.110	1.866	0.5515	FCC
$(U_{0.5}$ $La_{0.5})$ oxide	2.430	1.965	0.5529	FCC
$(U_{0.4}$ $La_{0.6})$ oxide	2.414	1.866	0.5542	FCC
$(U_{0.3}$ $La_{0.7})$ oxide	2.503	1.801	0.5556	FCC
$(U_{0.2}$ $La_{0.8})$ oxide	2.552	1.710	0.5569	FCC
$(U_{0.18}$ $La_{0.82})$ oxide	2.573	1.693	0.5572	FCC + HXL
$(U_{0.16}$ $La_{0.84})$ oxide	2.586	1.674	0.5572	FCC + HXL
$(U_{0.14}$ $La_{0.86})$ oxide	2.600	1.654	0.5571	FCC + HXL
$(U_{0.12}$ $La_{0.88})$ oxide	2.614	1.634	0.5571	FCC + HXL
$(U_{0.1}$ $La_{0.9})$ oxide	2.628	1.613	0.5572	FCC + HXL
Solid solution prepared by solid-state route				
$(U_{0.4}$ $La_{0.6})$ oxide	2.409	1.863	0.5543	FCC
$(U_{0.3}$ $La_{0.7})$ oxide	2.567	1.820	0.5552	FCC + HXL
$(U_{0.2}$ $La_{0.8})$ oxide	2.602	1.720	0.5552	FCC + HXL

FCC: Face centered cubic solid solution phase; HXL: Hexagonal lanthana phase.

solutions have a well-crystallized single-phase fluorite structure whereas hexagonal lanthana lines (HXL) are visible for y values larger than y = 0.82. The intensity of the HXL peak increases from y = 0.82 to 0.90. The observation is also substantiated by plot of

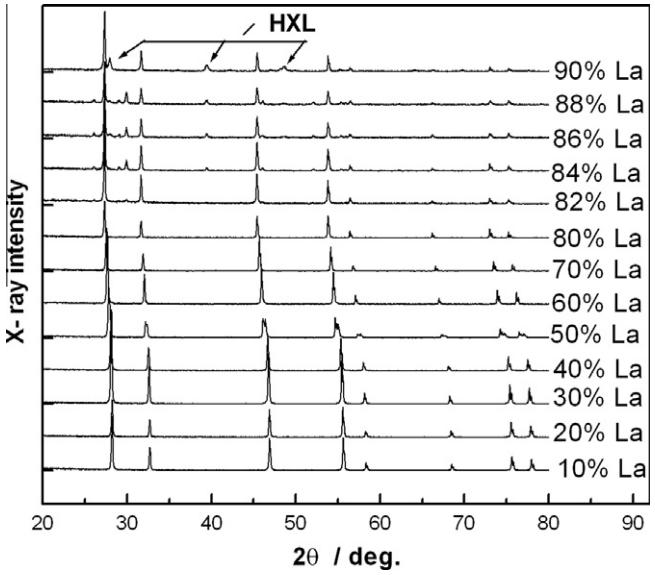

Fig. 1. Room temperature XRD pattern of $(U_{1-y}$ $La_y)$ $O_{2\pm x}$ prepared by combustion synthesis method.

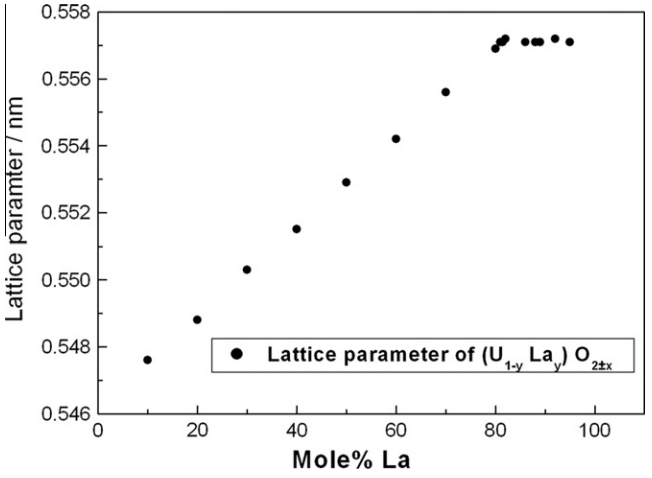

Fig. 2. Variation of lattice parameter with y for $(U_{1-y}$ $La_y)$ $O_{2\pm x}$.

lattice parameter against y as shown in Fig. 2. As seen from Fig. 2, the lattice parameter increases with increase in concentration of lanthanum oxide up to 80% and reaches a plateau. Therefore, it can be inferred that the solubility limit of lanthanum oxide in uranium oxide is in the region of y = 0.80–0.82. The solid solution with y = 0.82 was sintered further at 1873 K under flowing Ar + 8% H_2. The RTXRD analysis of the resultant sample also shows the presence of second phase HXL lines. This confirms the estimated solubility limit.

As seen from Table 3 and Fig. 2, the lattice parameter of $(U_{1-y}$ $La_y)$ $O_{2\pm x}$ increases with increase in the lanthanum content. In our earlier study [23] the room temperature lattice parameter (a) of $(U_{1-y}$ $Gd_y)$ $O_{2\pm x}$ was found to decrease with increase in Gd concentration. The ionic radii of U^{4+}, Gd^{3+}, and $La^{3+}$with eightfold co-ordination, are 0.1001 nm, 0.1053 nm and 0.1160 nm, respectively [26]. When U^{4+} is substituted with M^{3+} in the UO_2 lattice some of the U^{4+} is oxidized to either U^{5+} or U^{6+} in order to maintain electrical neutrality. The ionic radius of U^{5+} with eight fold co-ordination is 0.088 nm and that of U^{6+} is 0.086 nm [26]. The increase in lattice constant expected by doping with a cation of larger ionic radius is

overwhelmed by decrease in the average ionic radius of uranium ions due to oxidation, assuming a random distribution of the cations in the cation sub lattice. Therefore, a net negative change in the lattice constant on increase in dopant concentration is observed in the case of doping of UO_2 with Gd. However, in the case of $(U_{1-y}\ La_y)\ O_{2\pm x}$, since the ionic radius of La^{3+} is much larger than that of $U^{4+}$and the contribution of oxidation of U^{4+} to the decrease in the lattice parameter is less than the increase due to doping La ions, a net increase is observed.

The pseudo-binary phase diagram of $LaO_{1.5}$–UO_2 [27] shows that at 1873 K single-phase fluorite structure was observed up to a lanthanum oxide concentration of 72% whereas Diehl and Keller [7] and Kleykamp [11] reported that La_2O_3 is soluble in UO_2 up to 82 mol.% at 1523 K when heated under reducing atmosphere. They also reported [7,11] that the maximum solubility of lanthanum oxide in UO_2 to form stoichiometric mixed oxide is only 67 mol.%. In the oxidizing atmosphere the single phase region of the FCC solid solution $(U_{1-y}\ La_y)\ O_{2\pm x}$ is reported [6,7] to be in the range of $y = 0.25$–0.82 at 1823 K whereas, that in the reducing atmosphere is reported [6,7] in the range of $y = 0$–0.82 at 1523 K. However, when heated under vacuum condition Wilson et al. [8] reported the single phase FCC region in the range of $y = 0$–0.54 at 2023 K. Hill et al. [9] reported a single phase FCC region for $(U_{1-y}\ La_y)\ O_{2\pm x}$ at 2023 K under reducing atmosphere and that in vacuum is in the range of $y = 0$–0.75. Tagawa et al. [12] reported a single phase FCC region in the range of $y = 0.3$–0.45 and $y = 0.7$–0.9 when heated under oxidizing atmosphere at 1273 K. The results are consolidated and reported in a review article [6]. The present result is in agreement with that reported by Diehl and Keller [7] and Kleykamp [11].

Studies on solubility of lanthanum oxide in UO_2 by preparing the mixed oxide through solid-state route were carried out to determine whether the preparation route has an influence on the solubility. Three different solid solutions $(U_{1-y}\ La_y)\ O_{2\pm x}$ ($y = 0.6$–0.8) were prepared by solid-state route. The heat treatment conditions are maintained identical as those for the preparation by combustion route. XRD patterns of samples prepared by solid-state route were taken and are shown in Fig. 3. As can be seen in Fig. 3, the second phase of hexagonal lanthanum oxide is seen even for solid solution containing 70% La. This shows that the solid solubility limit of lanthanum oxide in urania is in the vicinity of 70%. This is also substantiated by the fact that the lattice parameter of solid solution (Table 3) with 70% lanthanum oxide is larger than

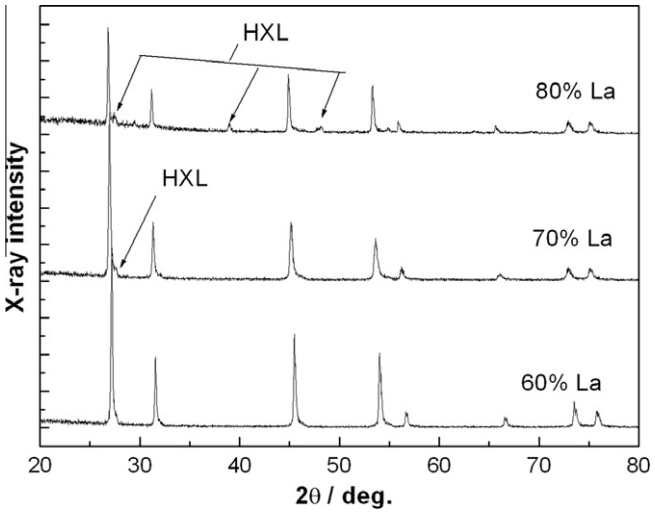

Fig. 3. Room temperature XRD pattern of $(U_{1-y}\ La_y)\ O_{2\pm x}$ prepared by solid state synthesis method.

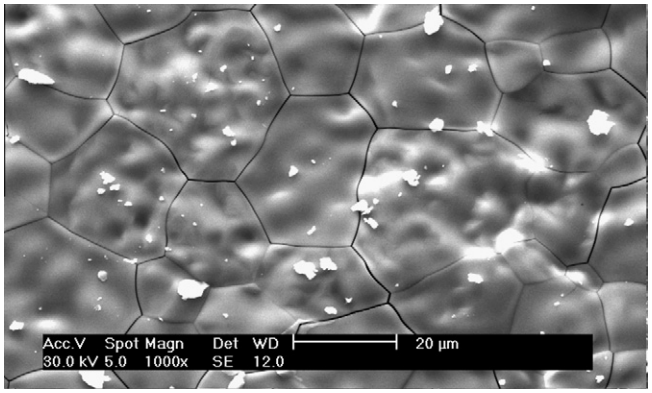

Fig. 4. SEM image of $(U_{0.4}\ La_{0.6})\ O_{1.87}$ prepared by combustion synthesis.

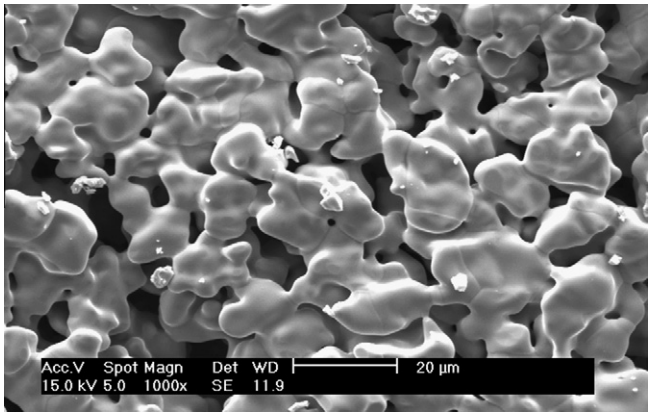

Fig. 5. SEM image of $(U_{0.4}\ La_{0.6})\ O_{1.86}$ prepared by solid-state synthesis.

that of 60% lanthanum oxide whereas that of 80% lanthanum oxide is, the same as that of 70% lanthanum oxide. The mixed oxide containing 70% lanthanum oxide was further sintered at 1873 K for 4 h under flowing Ar + 8% H_2. The RTXRD pattern of the resultant sample also shows the presence of second phase HXL. The higher observed solid-solubility of La in uranium dioxide prepared by combustion synthesis than that prepared by solid-state route under the same heat treatment conditions such as temperature, duration and atmosphere of heating is attributable to the fact that combustion synthesis, in general, yields materials of nm size and hence the kinetics of diffusion processes needed for the formation of solid solutions is expected to be favorable with reduction in grain size.

Figs. 4 and 5 show the SEM images of $(U_{0.4}\ La_{0.6})\ O_{2\pm x}$ prepared by combustion synthesis and solid-state route, respectively. As seen in the figures the solid solution prepared by combustion route crystallizes in a uniform grain size (≈20 μm) with well-defined grain boundaries, whereas the solid solution prepared by solid-state route is more porous, with neck formation and interconnected porosity. Figs. 6–8 show the SEM images of $(U_{1-y}\ La_y)\ O_{2\pm x}$ prepared by combustion route for $y = 0.80$, 0.82 and 0.90, respectively. As seen in the figures, the solid solution with $y = 0.80$ crystallizes with closed grain structures containing nano pores which are typical of a combustion method derived materials, whereas the solid solutions with $y = 0.82$ and 0.90 have flaky shaped materials whose grains are not properly formed. This result may be attributed to the precipitation of second phase (hexagonal lanthana), which is uniformly distributed throughout the matrix of the major phase. The observation is in good agreement with the investigation by XRD, which shows that the second phase of

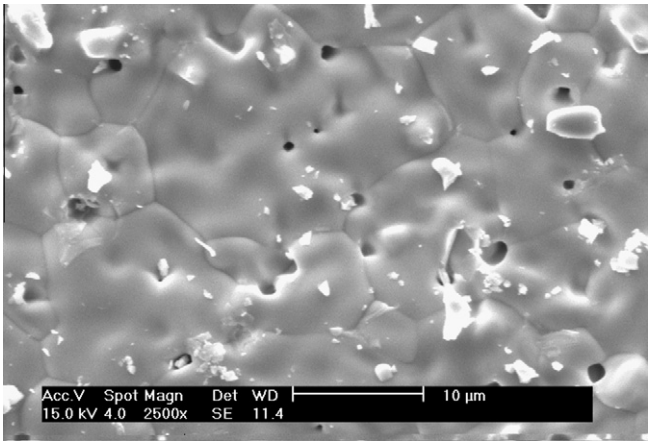

Fig. 6. SEM image of $(U_{0.2}\ La_{0.8})\ O_{1.71}$ prepared by combustion synthesis.

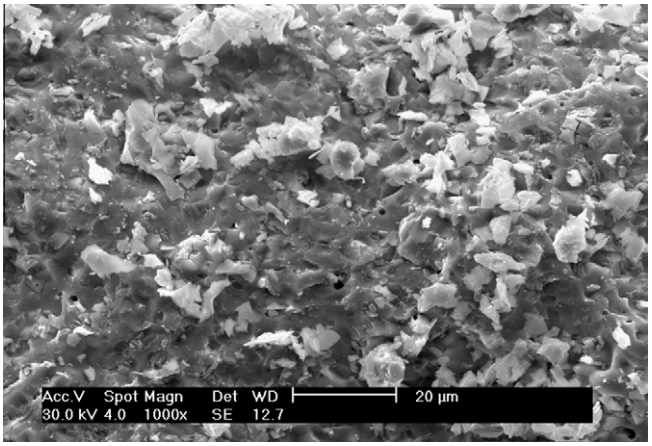

Fig. 7. SEM image of $(U_{0.18}\ La_{0.82})\ O_{1.69}$ prepared by combustion synthesis.

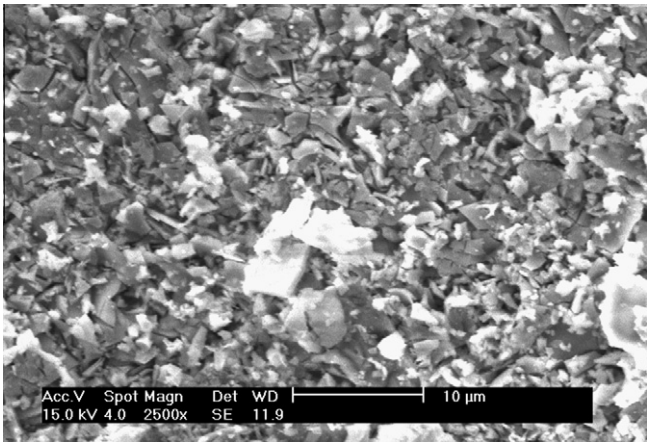

Fig. 8. SEM image of $(U_{0.1}\ La_{0.9})\ O_{1.61}$ prepared by combustion synthesis.

hexagonal lanthana was formed in the solid solution containing 82% lanthana.

3.3. Thermal expansion studies

UO_2 has face centered cubic (FCC) lattice while La_2O_3 has hexagonal structure. Thermal expansion characteristics of UO_2 and La_2O_3 were studied in our previous work [23,28]. The measured lattice parameters of $(U_{1-y}\ La_y)\ O_{2\pm x}$ (y = 0.2, 0.4, 0.6 and 0.8) as a function of temperature in the temperature range 298–1973 K are shown in Fig. 9 and are also listed in Tables 4 and 5. The variation of lattice parameters, a (nm) with temperature (K) for $(U_{1-y}\ La_y)\ O_{2\pm x}$ (y = 0.2, 0.4, 0.6 and 0.8) was fitted to a second order polynomial in the temperature interval (T-298) by least squares method and are given by the following expressions in the temperature range 298–1973 K.

$$a(\mathrm{nm})[(U_{0.8}\ La_{0.2})O_{1.95}] = 0.54771 + 3.2649\times10^{-6}(T\text{-}298) + 1.6320\times10^{-9}(T\text{-}298)^2 \quad (1)$$

$$a(\mathrm{nm})[(U_{0.6}\ La_{0.4})O_{1.87}] = 0.55036 + 3.4976\times10^{-6}(T\text{-}298) + 1.6920\times10^{-9}(T\text{-}298)^2 \quad (2)$$

$$a(\mathrm{nm})[(U_{0.4}\ La_{0.6})O_{1.87}] = 0.55302 + 3.7324\times10^{-6}(T\text{-}298) + 1.7543\times10^{-9}(T\text{-}298)^2 \quad (3)$$

$$a(\mathrm{nm})[(U_{0.2}\ La_{0.8})O_{1.71}] = 0.55567 + 3.9694\times10^{6}(T\text{-}298) + 1.8163\times10^{-9}(T\text{-}298)^2 \quad (4)$$

From the above relations instantaneous (α_i) and mean (α_m) linear thermal expansion coefficients are computed as given below and are also given in Tables 4 and 5.

$$\alpha_i - \text{instantaneous} = (1/a_T)(da_T/dT) \quad (5)$$

$$\alpha_m - mean = (1/a_{298}) \times (a_T - a_{298})/(T\text{-}298) \quad (6)$$

Eqs. (1)–(4) were used to calculate the mean linear thermal expansions of the respective mixed oxides which are presented in Tables 4 and 5, the result of which is shown in Fig. 10. From the variation of lattice parameters with temperature, % linear thermal expansion were computed and fitted to the following polynomials of temperature by least squares method. As seen in Fig. 10, the percentage thermal expansion of $(U_{1-y}\ La_y)\ O_{2\pm x}$ increases with increase in the lanthanum content (temperature range 298–1973 K).

$$\text{Thermal expansion } (\%)[(U_{0.8}La_{0.2})O_{1.95}] = -0.19845 + 5.96401\times10^{-4}T + 2.96141\times10^{-7}T^2 \quad (7)$$

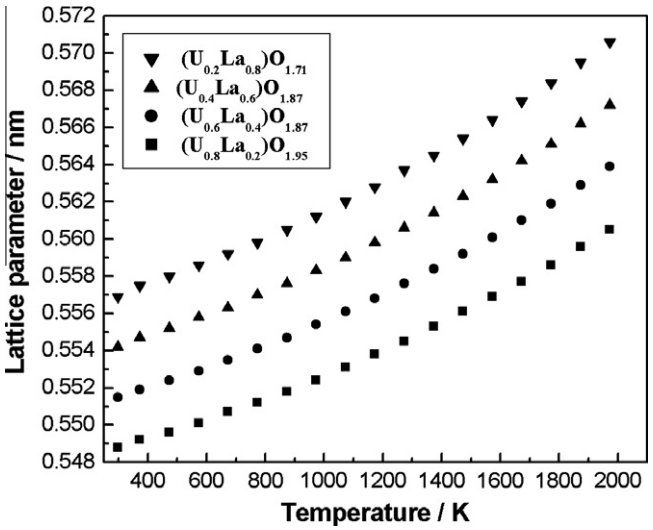

Fig. 9. Lattice parameter as a function of temperature of $(U_{1-y}\ La_y)\ O_{2\pm x}$.

Table 4
HTXRD data of uranium–lanthanum solid solutions.

T/K	$(U_{0.8}La_{0.2})\ O_{1.95}$				$(U_{0.6}\ La_{0.4})\ O_{1.87}$			
	a/nm	TE/%	$\alpha_i/10^{-6}\ K^{-1}$	$\alpha_m/10^{-6}\ K^{-1}$	a/nm	TE/%	$\alpha_i/10^{-6}\ K^{-1}$	$\alpha_m/10^{-6}\ K^{-1}$
298	0.5488	0.00	7.72	7.72	0.5515	0.00	8.17	8.17
373	0.5492	0.07	8.16	8.17	0.5519	0.08	8.63	8.63
473	0.5496	0.15	8.75	8.76	0.5524	0.17	9.23	9.25
573	0.5501	0.24	9.33	9.36	0.5529	0.26	9.83	9.86
673	0.5507	0.34	9.92	9.95	0.5535	0.36	10.44	10.47
773	0.5512	0.44	10.50	10.55	0.5541	0.47	11.04	11.09
873	0.5518	0.55	11.08	11.14	0.5547	0.58	11.63	11.70
973	0.5524	0.66	11.66	11.74	0.5554	0.70	12.23	12.32
1073	0.5531	0.78	12.24	12.33	0.5561	0.83	12.82	12.93
1173	0.5538	0.91	12.81	12.93	0.5568	0.96	13.41	13.54
1273	0.5545	1.04	13.38	13.52	0.5576	1.10	14.00	14.16
1373	0.5553	1.18	13.95	14.12	0.5584	1.24	14.59	14.77
1473	0.5561	1.32	14.52	14.71	0.5592	1.39	15.17	15.39
1573	0.5569	1.47	15.08	15.30	0.5601	1.55	15.75	16.00
1673	0.5577	1.63	15.64	15.90	0.5610	1.71	16.33	16.61
1773	0.5586	1.79	16.20	16.49	0.5619	1.88	16.91	17.23
1873	0.5596	1.96	16.76	17.09	0.5629	2.06	17.48	17.84
1973	0.5605	2.13	17.31	17.68	0.5639	2.24	18.05	18.45

TE – Thermal expansion.

Table 5
HTXRD data of uranium–lanthanum solid solutions.

T/K	$(U_{0.4}\ La_{0.6})\ O_{1.87}$				$(U_{0.2}\ La_{0.8})\ O_{1.71}$			
	a/nm	TE/%	$\alpha_i/10^{-6}\ K^{-1}$	$\alpha_m/10^{-6}\ K^{-1}$	a/nm	TE/%	$\alpha_i/10^{-6}\ K^{-1}$	$\alpha_m/10^{-6}\ K^{-1}$
298	0.5542	0.00	8.62	8.62	0.5569	0.00	9.07	9.07
373	0.5547	0.09	9.09	9.10	0.5575	0.10	9.55	9.56
473	0.5552	0.18	9.71	9.73	0.5580	0.20	10.19	10.21
573	0.5558	0.28	10.33	10.36	0.5586	0.30	10.83	10.87
673	0.5563	0.39	10.95	11.00	0.5592	0.41	11.47	11.52
773	0.5570	0.50	11.57	11.63	0.5598	0.53	12.11	12.17
873	0.5576	0.62	12.19	12.26	0.5605	0.65	12.74	12.82
973	0.5583	0.74	12.80	12.89	0.5612	0.78	13.37	13.47
1073	0.5590	0.87	13.41	13.53	0.5620	0.92	14.00	14.13
1173	0.5598	1.01	14.02	14.16	0.5628	1.06	14.62	14.78
1273	0.5606	1.15	14.63	14.79	0.5637	1.21	15.25	15.43
1373	0.5614	1.31	15.23	15.43	0.5645	1.37	15.87	16.08
1473	0.5623	1.46	15.83	16.06	0.5654	1.53	16.48	16.74
1573	0.5632	1.63	16.43	16.69	0.5664	1.71	17.10	17.39
1673	0.5642	1.80	17.02	17.33	0.5674	1.88	17.71	18.04
1773	0.5651	1.98	17.61	17.96	0.5684	2.07	18.31	18.69
1873	0.5662	2.16	18.20	18.59	0.5695	2.26	18.92	19.35
1973	0.5672	2.35	18.78	19.23	0.5706	2.46	19.52	20.00

TE – Thermal expansion.

$$\text{Thermal expansion } (\%)[(U_{0.6}La_{0.4})O_{1.87}] = -0.20464 + 6.33107 \times 10^{-4}T + 3.0661 \times 10^{-7}T^2 \quad (8)$$

$$\text{Thermal expansion } (\%)[(U_{0.4}La)_{0.6})O_{1.87}] = -0.21216 + 6.71182 \times 10^{-4}T + 3.1767 \times 10^{-7}T^2 \quad (9)$$

$$\text{Thermal expansion } (\%)[(U_{0.2}La_{0.8})O_{1.71}] = -0.21835 + 7.07888 \times 10^{-4}T + 3.28139 \times 10^{-7}T^2 \quad (10)$$

The coefficients of thermal expansion for $(U_{1-y}\ La_y)\ O_{2\pm x}$ (y = 0.2, 0.4, 0.6, 0.8) in the temperature range 298–1973 K determined are 17.7, 18.5, 19.2 and 20.0 $\times\ 10^{-6}\ K^{-1}$ respectively. The coefficients of thermal expansion increase with increase of lanthanum content in $(U_{1-y}\ La_y)\ O_{2\pm x}$. This is because when U^{4+} ion is replaced by La^{3+} ion in the UO_2 lattice, the bond strength is decreased as the La^{3+}–O^{2-} interaction is weaker than that of U^{4+}–O^{2-}. Therefore the anharmonicity of the mixed oxide increases with increase in the

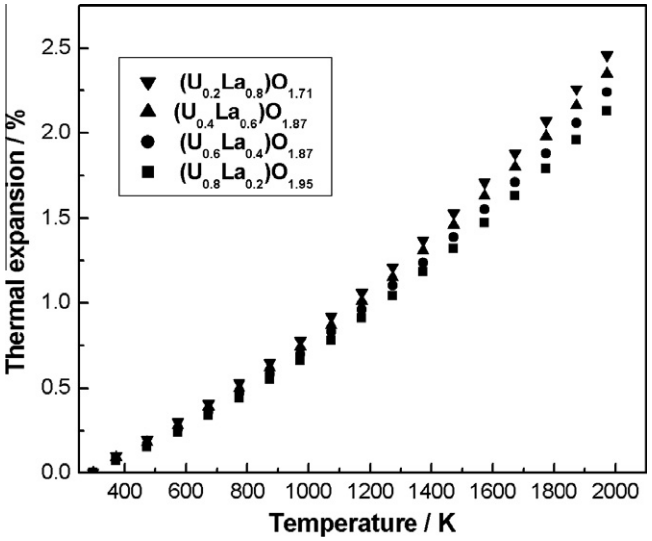

Fig. 10. Thermal expansion data of $(U_{1-y}\ La_y)\ O_{2\pm x}$.

concentration of dopant La^{3+}. Larger the anharmonicity higher will be the thermal expansion.

4. Conclusion

Uranium–lanthanum mixed oxide solid solutions were prepared by combustion synthesis to ascertain the solubility of $LaO_{1.5}$ in UO_2 at 1873 K. Single-phase fluorite structure was observed for $(U_{1-y}\ La_y)\ O_{2\pm x}$ up to $y = 0.82$ for the solid solutions prepared by combustion synthesis whereas for those prepared by solid-state route the solubility of $LaO_{1.5}$ in UO_2 was around 70%. Higher observed solid solubility for the solid solutions prepared by combustion synthesis than that prepared by solid-state route under the same heat treatment conditions such as temperature, duration of heating and atmosphere of heating may be due to the fact that combustion synthesis, in general yields materials of nm size and the kinetics of diffusion process needed for the formation of solid solutions is expected to be favorable with reduction in grain size. Thermal expansion characteristics of $(U_{1-y}\ La_y)\ O_{2\pm x}$ were studied by using HTXRD. The thermal expansion data of uranium–lanthanum mixed oxides are reported for the first time. The percentage thermal expansion of $(U_{1-y}\ La_y)\ O_{2\pm x}$ increases with increase in the lanthanum content.

References

[1] H. Kleykamp, J. Nucl. Mater. 131 (1985) 221–246.
[2] E.H.P. Cordfunke, R.J.M. Konings, J. Nucl. Mater. 152 (1988) 301–309.
[3] K. Une, M. Oguma, J. Nucl. Mater. 115 (1983) 84–90.
[4] A.M. Diness, B. Rustam, J. Mater. Sci. 4 (1969) 613–624.
[5] P.S. Murti, C.K. Mathews, High Temp. High Press. 22 (1990) 379–382.
[6] L.R. Morss, N.M. Edelstein, J. Fuger, J.J. Katz (Eds.), The Chemistry of the Actinide and Transactinide Elements, third ed., vol. 1, Springer, 2006.
[7] H.G. Diehl, C. Keller, J. Solid, State Chem. 3 (1971) 621–636.
[8] W.B. Wilson, C.A. Alexander, A.F. Gerds, J. Inorg. Nucl. Chem. 20 (1961) 242–251.
[9] D.C. Hill, J.H. Handwerk, R.J. Beals, Argonne National Laboratory Report, 1963, ANL-6711.
[10] E. Stadlbauer, U. Wichmann, U. Lott, C. Keller, J. Solid, State Chem. 10 (1974) 341–350.
[11] H. Kleykamp, J. Nucl. Mater. 206 (1993) 82–86.
[12] H. Tawaga, T. Fujino, K. Ouchi, K. Watanabe, K. Saita, J. Nucl. Sci. Tech. 20 (6) (1983) 467–474.
[13] S.S. Manoharan, K.C. Patil, J. Am. Ceram. Soc. 75 (1992) 1012–1015.
[14] M. Muthuraman, Bull. Mater. Sci. 17 (1994) 977–987.
[15] T. Ye, Z. Guiwen, Z. Weiping, X. Shangda, Mater. Res. Bull. 32 (1997) 501–506.
[16] D.A. Fumo, M.R. Morelli, A.M. Segadaes, Mater. Res. Bull. 31 (1996) 1243–1255.
[17] V. Chandramouli, S. Anthonysamy, P.R. Vasudeva Rao, J. Nucl. Mater. 265 (1999) 255–261.
[18] J-G. Lee, H. Mori, H. Yasuda, Phys. Rev. B 65 (2002) 1–4.
[19] J-G. Lee, H. Mori, H. Yasuda, Phys. Rev. B 66 (2002) 1–4.
[20] J-G. Lee, H. Mori, Phys. Rev. Lett. 93 (2004) 1–4.
[21] G. Ouyang, X. Tan, C.X. Wang, G. Wyang, Nanotechnology 17 (2006) 4257–4262.
[22] R. Venkata Krishnan, K. Nagarajan, Thermochim. Acta 440 (2006) 141–145.
[23] R. Venkata Krishnan, G. Panneerselvam, P. Manikandan, M.P. Antony, K. Nagarajan, J. Nucl. Radiochem. Chem. Sci. 10 (1) (2009) 19–26.
[24] Powder diffraction files (Inorganic Phases), Joint Committee on Powder Diffraction Data (JCPDS), International Centre for Diffraction Data (1999). (ICDD Card Number: 05-0602).
[25] Powder diffraction files (Inorganic Phases), Joint Committee on Powder Diffraction Data (JCPDS), International Centre for Diffraction Data (1999). (ICDD Card Number: 41-1422).
[26] R.D. Shannon, Acta Cryst. A32 (1976) 751–767.
[27] C.W. Bale, P. Chartrand, S.A. Decterov, G. Eriksson, K. Hack, R. Ben Mahfoud, J. Melançon, A.D. Pelton, S. Petersen, Calphad 62 (2002) 189–228.
[28] G. Panneerselvam, M.P. Antony, in: Proceedings of 14th National Symposium on Thermal Analysis, Baroda, India, 10–22 January 2004, pp. 95–97.